

Supplementary Materials for
Collecting the space distributed Maxwell's displacement current for ultrahigh
electrical density of TENG through 3D fractal structure design

Li Ang Zhang[#], Shuhai Liu[#], Juan Wen, Xiaoqing Huo, Bolang Cheng, Zhiyi Wu,
Longfei Wang, Yong Qin*, and Zhong Lin Wang**

[#] These authors contribute equally to this work.

*Corresponding author. E-mail: lfwang12@binn.cas.cn, qinyong@lzu.edu.cn,

zhong.wang@mse.gatech.edu.

This file includes:

Materials and Methods

Supplementary Notes 1-2

Supplementary Figures 1-13

Supplementary Movies 1-5

Materials and Methods

Fabrication of the FSNG.

(1) An acrylic plate (thickness of 5 mm) with a columnar embossment ($10 \times 1 \times 2 \text{ cm}^3$) is prepared as the base.

(2) Two pieces of Ag ($3 \times 3 \text{ cm}^2$) as electrodes are fabricated on the surface of commercial PET tape (thickness of 10 μm) by magnetron sputtering technology. The detail parameters are controlled at pressure of 0.5 Pa, Ar gas of 30 sccm, DC power of 50 W, time of 8 min. PET tapes with electrodes layer are prepared by repeated magnetron sputtering.

(3) Use the treated tape to stick on the acrylic base. Then two copper wires are fixed on the base. One end of the copper wires is connected with the Ag electrodes respectively, the other end of the copper wires is fixed on the upper half part and lower half part of the side of the columnar embossment, respectively.

(4) Another treated tape is taped right above the first tape layer. Similarly, another two copper wires are fixed on the base. One end of the copper wires is connected with the Ag electrodes above the second tape layer respectively. The other end of the copper wires is fixed on the lower half part and upper half part of the side of the columnar embossment respectively, which is contrary to that in step (3).

(5) Repeat the step (3) and (4) alternately. Fabrication of the FSNG with n units needs to tape n layers of the PET with Ag electrodes ($n = 4, 14$ and 40). For the fractal structure with 40 units, the thickness would be 400 μm .

(6) The diodes are connected between each unit.

(7) The commercial PTFE film (80 μm) is taped on the right top of the treated PET tapes, as one triboelectric layer.

(8) As another triboelectric layer, a PU foam ($3 \times 3 \times 0.1 \text{ cm}^3$) adhered on the center of square acrylic plate. Then, two strips of conductive fabric are fixed on the upper half part and lower half part of the side of the square plate. The size of the square plate is precisely designed. When the PU foam slides on the top of right electrode area, the side of plate just contacts with the side of columnar embossment. Meanwhile, the conductive fabric strips mechanically connect with the ends of copper

wires, forming the structure of mechanical motion switches.

Electrical measurement and characterization.

The sliders of FSNG and classical triboelectric nanogenerator are driven by a linear motor (LinMot, PS01-37×120-C). The open-circuit voltage of the triboelectric nanogenerator is measured by electrometer (Keithley 6514) with series resistance voltage division method. The short-circuit current, load current and output charge of triboelectric nanogenerator are measured by electrometer (Keithley 6514). The open-circuit voltage of FSNG is measured by an oscilloscope (Tektronix, MDO 3024). The circuit for measuring the load current of FSNG is shown in **Fig. S12**. The load current higher than 1 mA is calculated from the voltage divided by resistance and the voltage is measured by an oscilloscope (Tektronix, MDO 3024). The load current lower than 1 mA is measured by an electrometer (Keithley 6514, current measuring range: 0-10 mA). The circuit for measuring the output charge of FSNG is shown in **Fig. S13**. The output charge higher than 20 μC is calculated from the voltage of the electrolytic capacitor with capacitance of 10 μF , and the voltage is measured by an electrometer (Keithley 6514). The output charge lower than 20 μC is directly measured by an electrometer (Keithley 6514, charge measuring range: 0-20 μC).

Supplementary Note 1. The detail parameters of simulation.

For the classical triboelectric nanogenerator, the materials from top to bottom are polyurethane (relative dielectric constant of 3), polytetrafluoroethylene (relative dielectric constant of 2.6), two silver films (conduction). And the sizes are 21*2.5 mm², 45*2.5 mm², 21*1 mm², 21*1 mm², respectively. The electrification positive charge is set as 100 μC/m on the bottom surface of polyurethane, and the electrification negative charge is set as 50 μC/m on the top surface of polytetrafluoroethylene.

For the FSNG, the top few materials and sizes are the same with above triboelectric nanogenerator. The difference is that there are multiple silver electrode layers and each two electrodes are connected by diode respectively. And the polyethylene terephthalate (relative dielectric constant of 3.64, size of 45*2.5 mm²) is filled between each two adjacent electrode layers. In addition, the electrification charge is the same with that of the triboelectric nanogenerator above.

Supplementary Note 2. The output power is calculated by the formula $W=I^2 R$, and the output energy is calculated by the formula $E=I^2 Rt$.

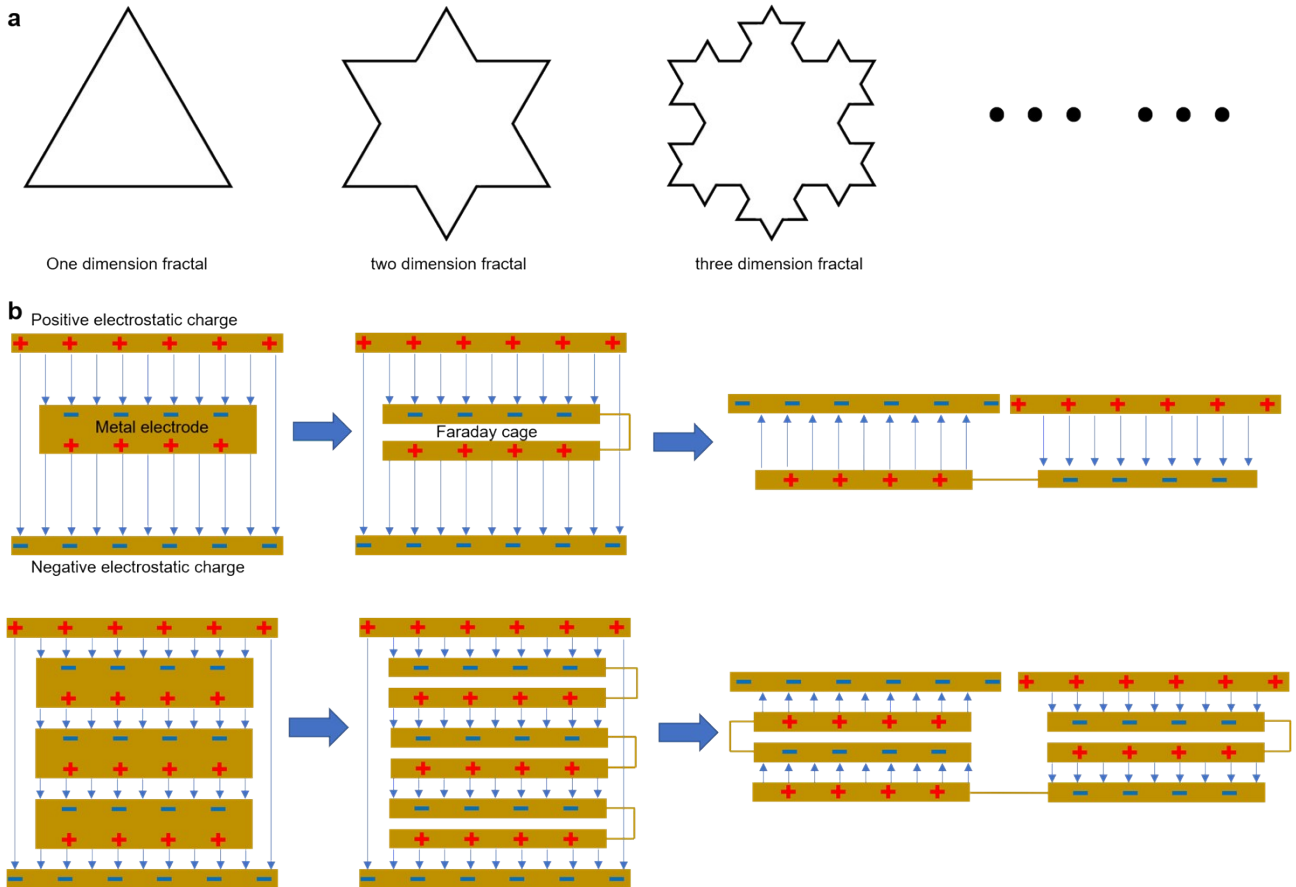


Fig. S1. a, Schematics of a fractal structure. **b**, The Faraday cage theory in the classical TENG and the structure combined fractal effect and Faraday cage theory which could collect the Maxwell's displacement current more finely and efficiently.

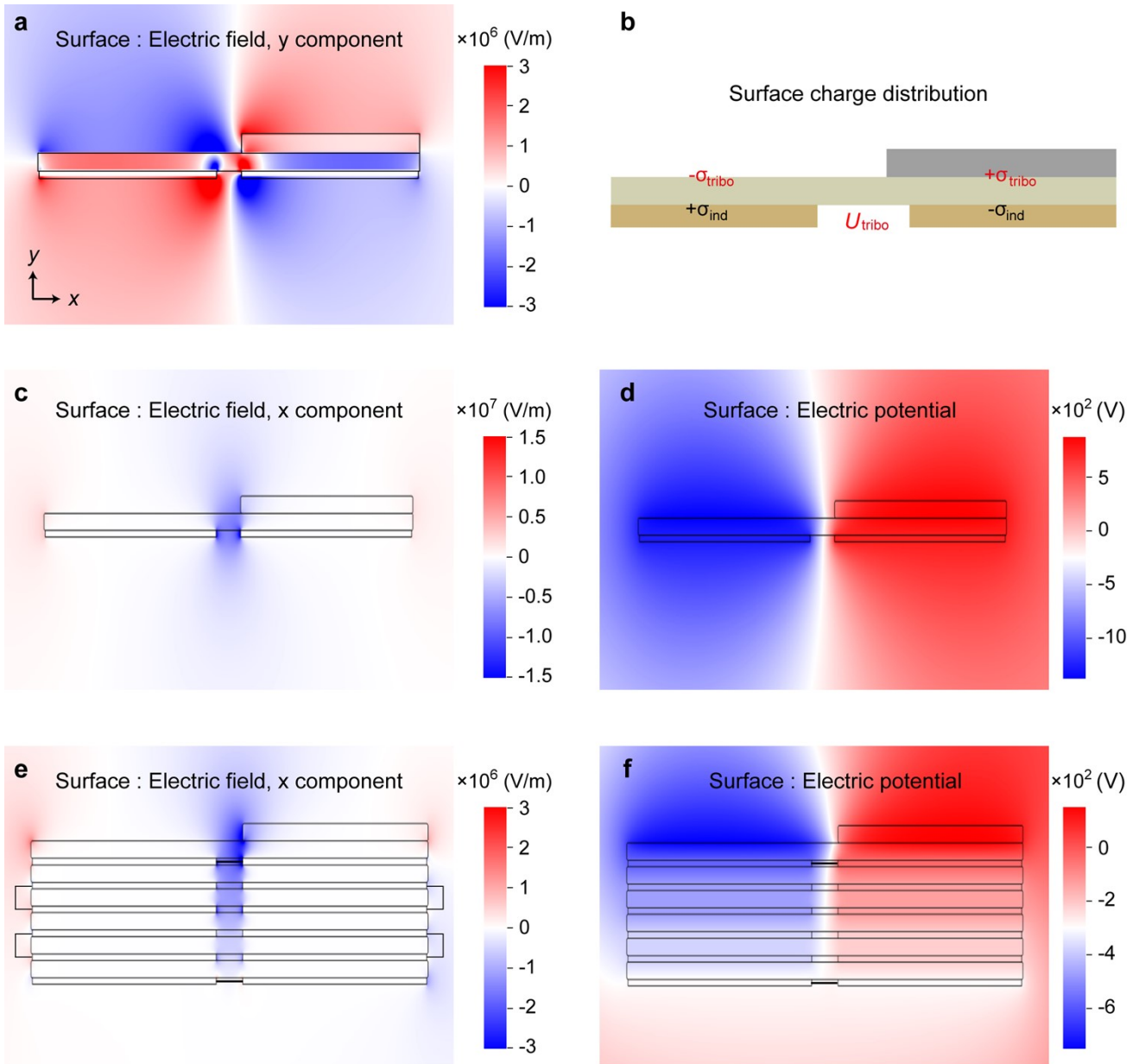


Fig. S2. Theoretical simulation of electric field distribution and potential distribution of the FSNG and a classical TENG. a, The electric field distribution (y component) of classical TENG. **b,** The schematic diagram of induced charge distribution in the electrodes of a classical TENG. **c,** The electric field distribution (x component) of a classical TENG. **d,** The electric potential distribution of a classical TENG. **e,** The electric field distribution (x component) of the FSNG. **f,** The electric potential distribution of the FSNG.

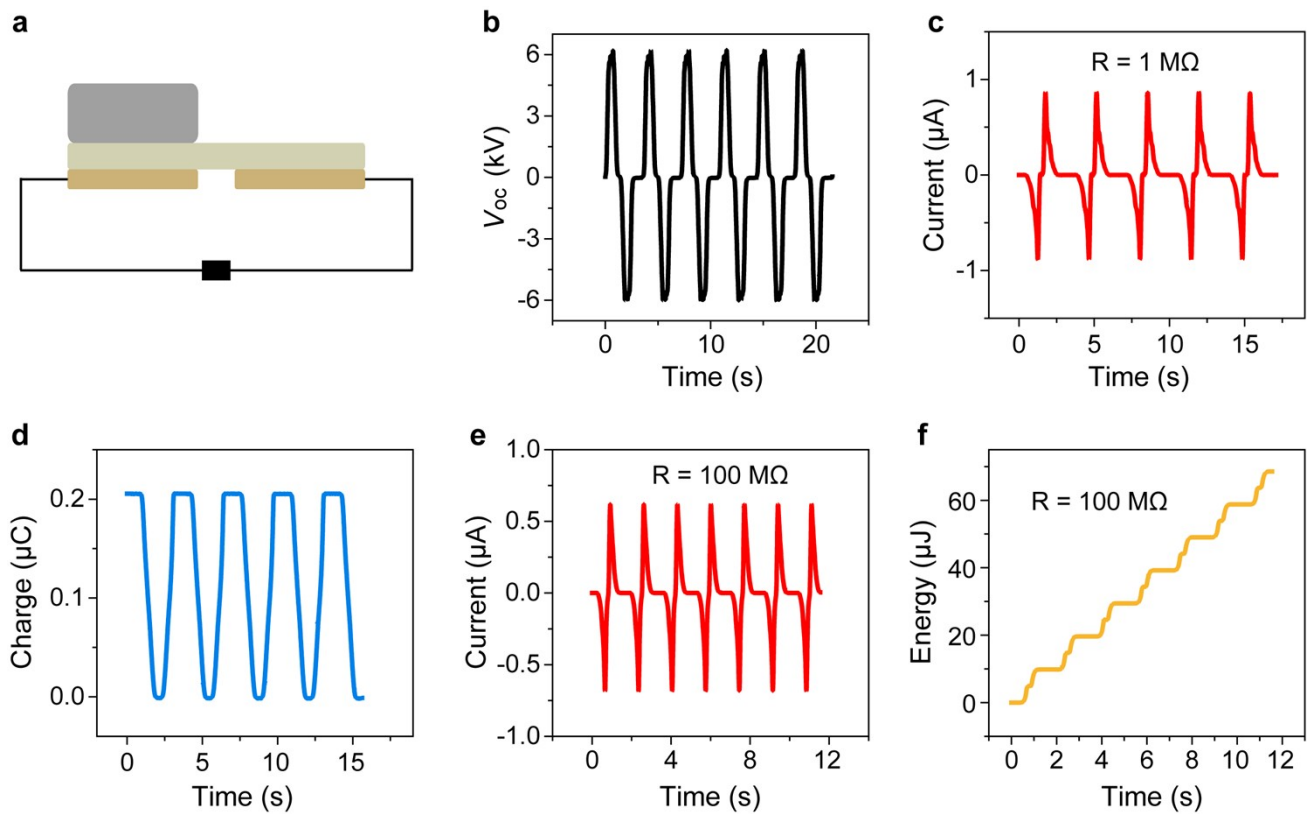


Fig. S3. Output performance of a classical TENG with the same triboelectric materials of the FSNG. **a**, Schematic diagram of the TENG. **b**, The open-circuit voltage, **(c)** The output current (load resistance of $1\text{ M}\Omega$), **(d)** The output charge, **(e)** The output current (load resistance of $100\text{ M}\Omega$), **(f)** The output energy (load resistance of $100\text{ M}\Omega$) of the TENG, which is calculated by the output current (load resistance of $100\text{ M}\Omega$). Compared with the classical TENG, the FSNG has manyfold increasing output current, charge, energy and the manyfold decreasing output voltage.

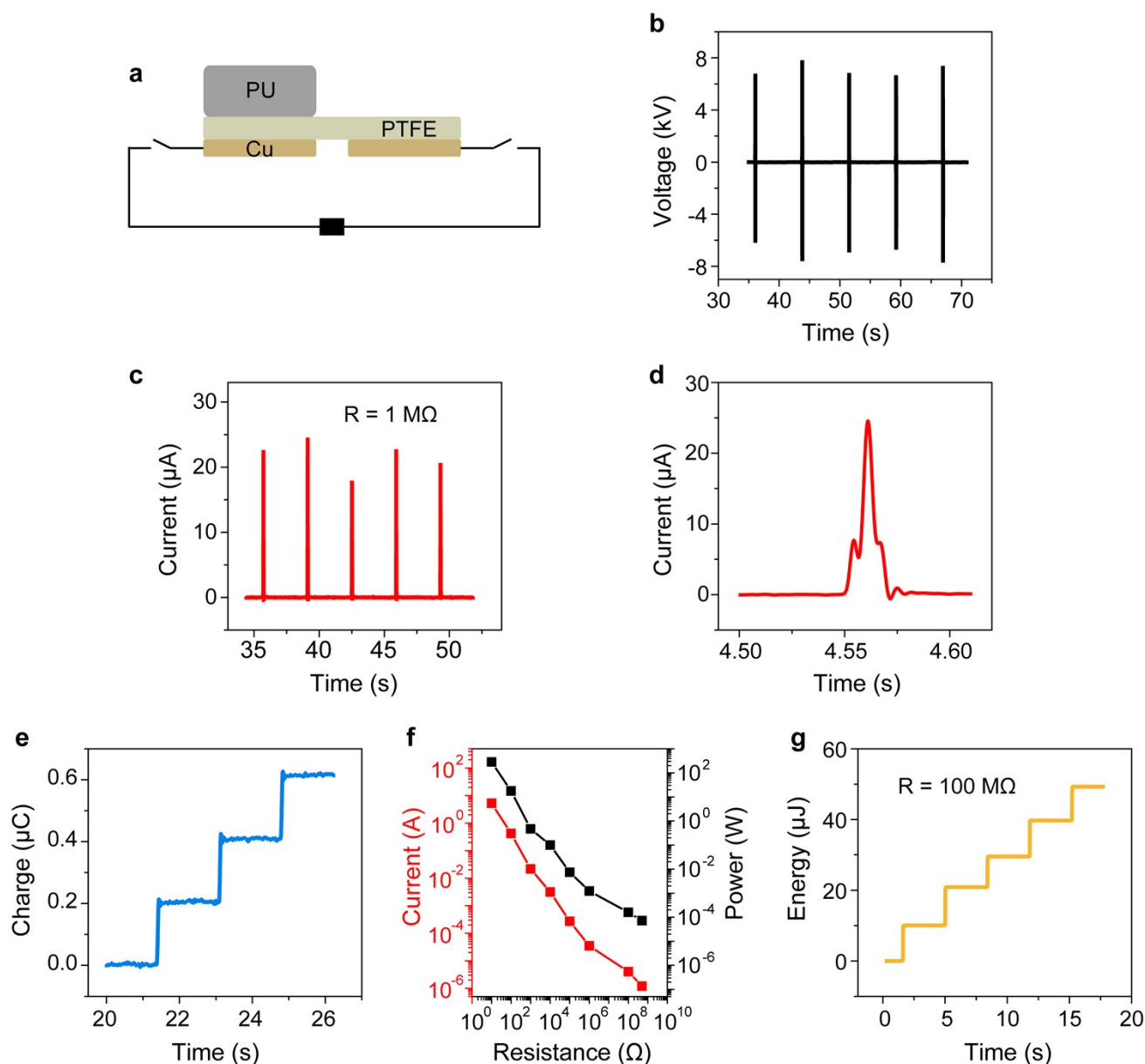


Fig. S4. Output performance of the TENG with motion switch structure (control group). **(a)**, Schematic of the TENG with motion switch structure. **(b)** Open-circuit voltage, **(c)** Output current (load resistance R of $1\text{ M}\Omega$) and **(d)** its enlarged curve, which demonstrates the time of output process is about 0.02 s , **(e)** Output charge of TENG with motion switch. **(f)** Instantaneous current and power of TENG with motion switch depending of load resistance. **(g)** Output energy of TENG with motion switch (load resistance R of $100\text{ M}\Omega$).

Compared with the classical TENG, only the output peak current and instantaneous power are higher, and all other output performances (voltage, charge and energy) are the same. And the high output instantaneous current and power is achieved by reducing the time of output process. Compared with the time of output process of classical TENG (about 0.5 s), the time of output process reduces to 0.02 s . In addition, compared with the FSNG, the control group shows greatly higher output voltage and lower output current, charge, power and energy density. The comparison

of the classical TENG, control group and FSNG demonstrates the manifold output performance of the FSNG are not caused by the motion switch structure.

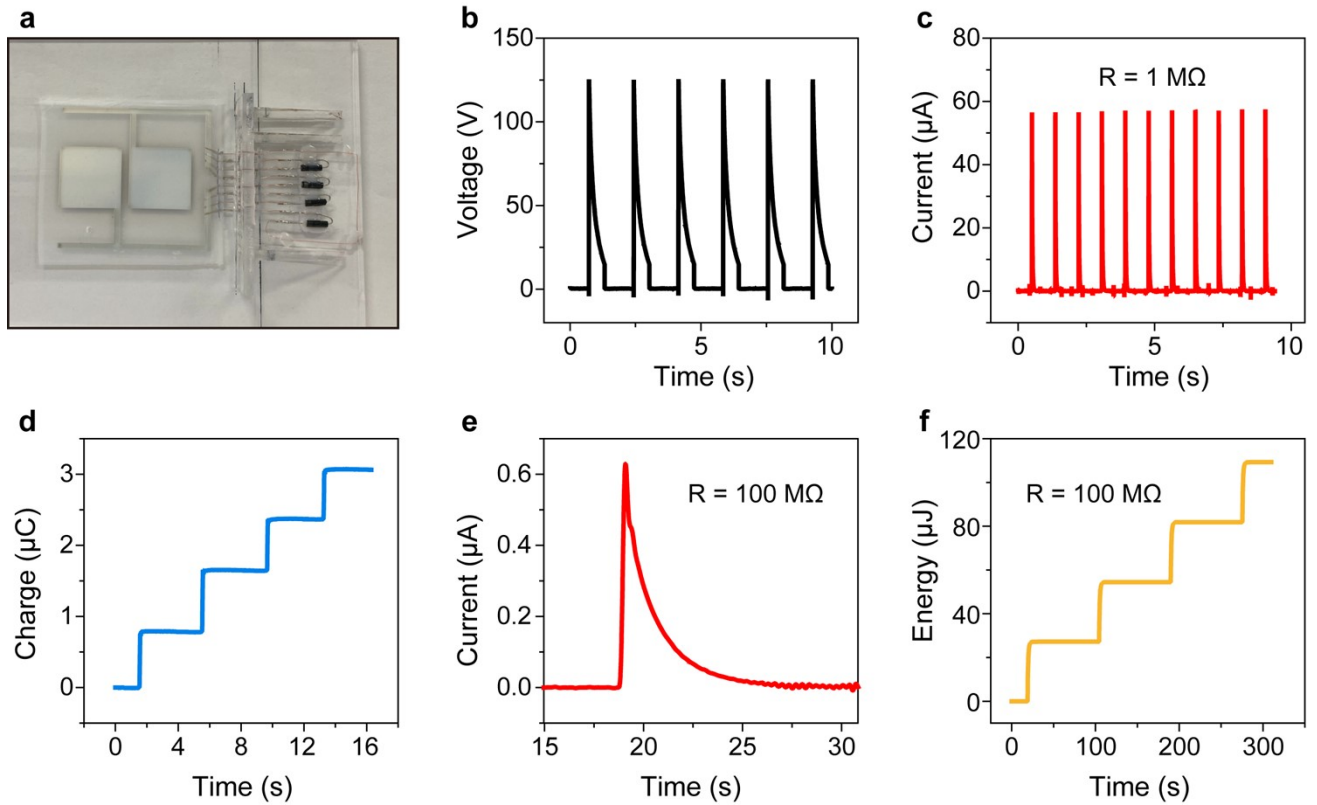


Fig. S5. Output performance of the FSNG with 4 fractal units. **a**, Optical photograph of the FSNG. **b**, Open-circuit voltage, **(c)** Output current (load resistance R of $1 \text{ M}\Omega$), **(d)** Output charge, **(e)** Output current (load resistance R of $100 \text{ M}\Omega$), and **(f)** Output energy (load resistance R of $100 \text{ M}\Omega$) of the FSNG with 4 fractal units.

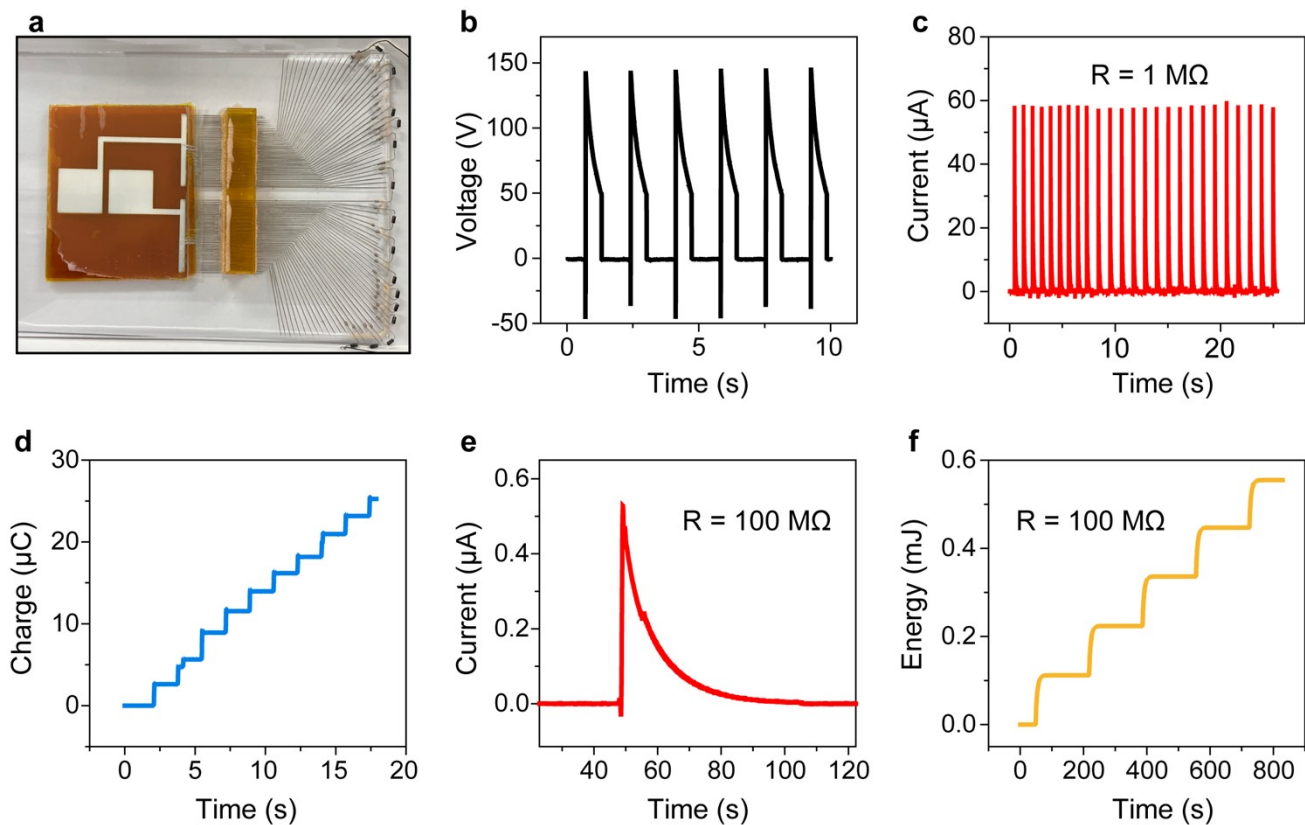


Fig. S6. Output performance of the FSNG with 14 fractal units. **a**, Optical photograph of the FSNG with 14 fractal units. **(b)** Open-circuit voltage, **(c)** Output current (load resistance R of $1 \text{ M}\Omega$), **(d)** Output charge, **(e)** Output current (load resistance R of $100 \text{ M}\Omega$), and **(f)** Output energy (load resistance R of $100 \text{ M}\Omega$) of the FSNG with 14 fractal units.

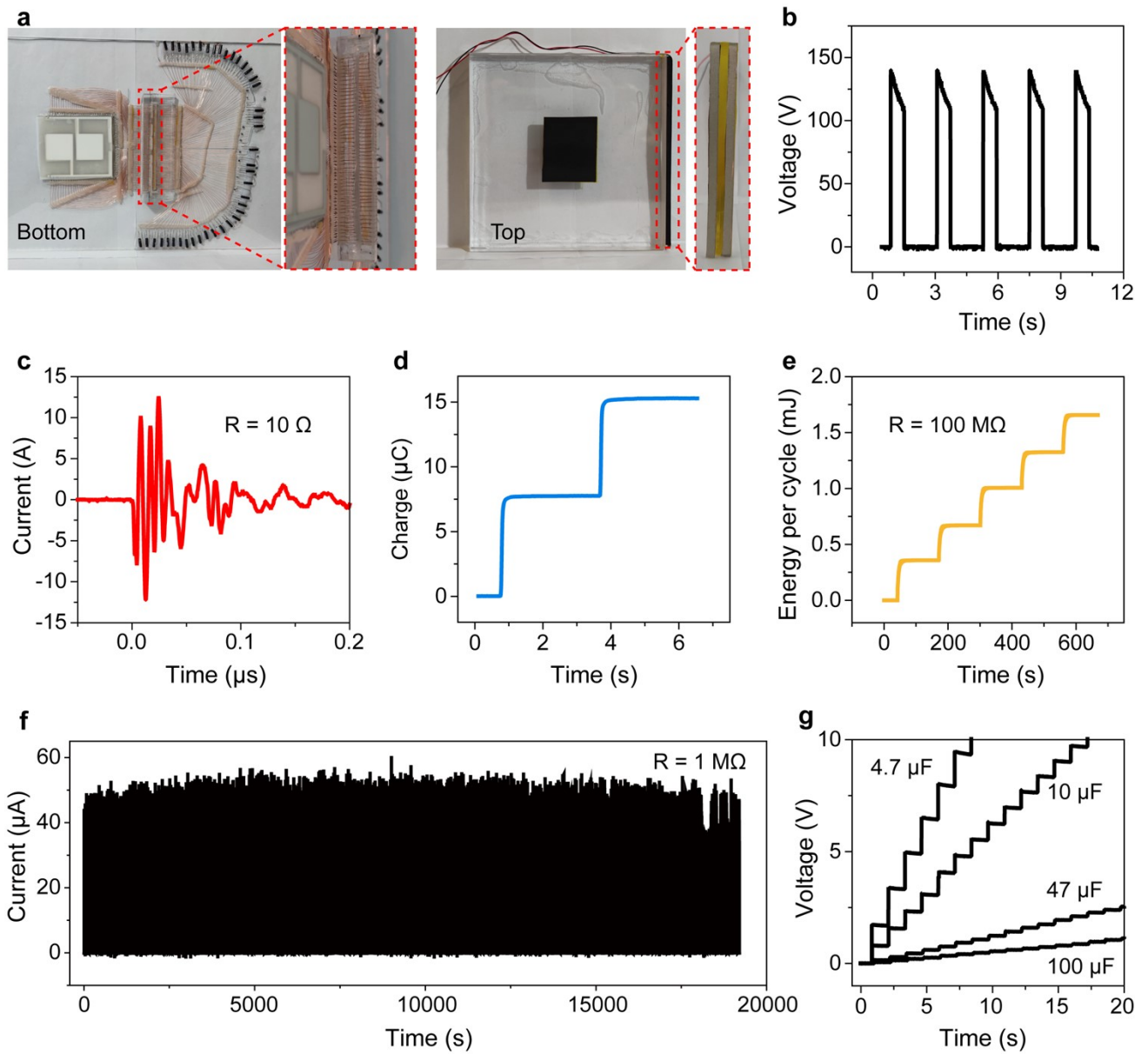


Fig. S7. Output performance of the FSNG with 40 fractal units. (a), Optical photograph of the FSNG with 40 fractal units. (b) Open-circuit voltage, (c) Output current (load resistance R of 10Ω), (d) Output charge, (e) Output energy, and (f) Long-term stability of the FSNG with 40 fractal units. (g), Voltages of the electrolytic capacitors with different capacitance charging by the FSNG.

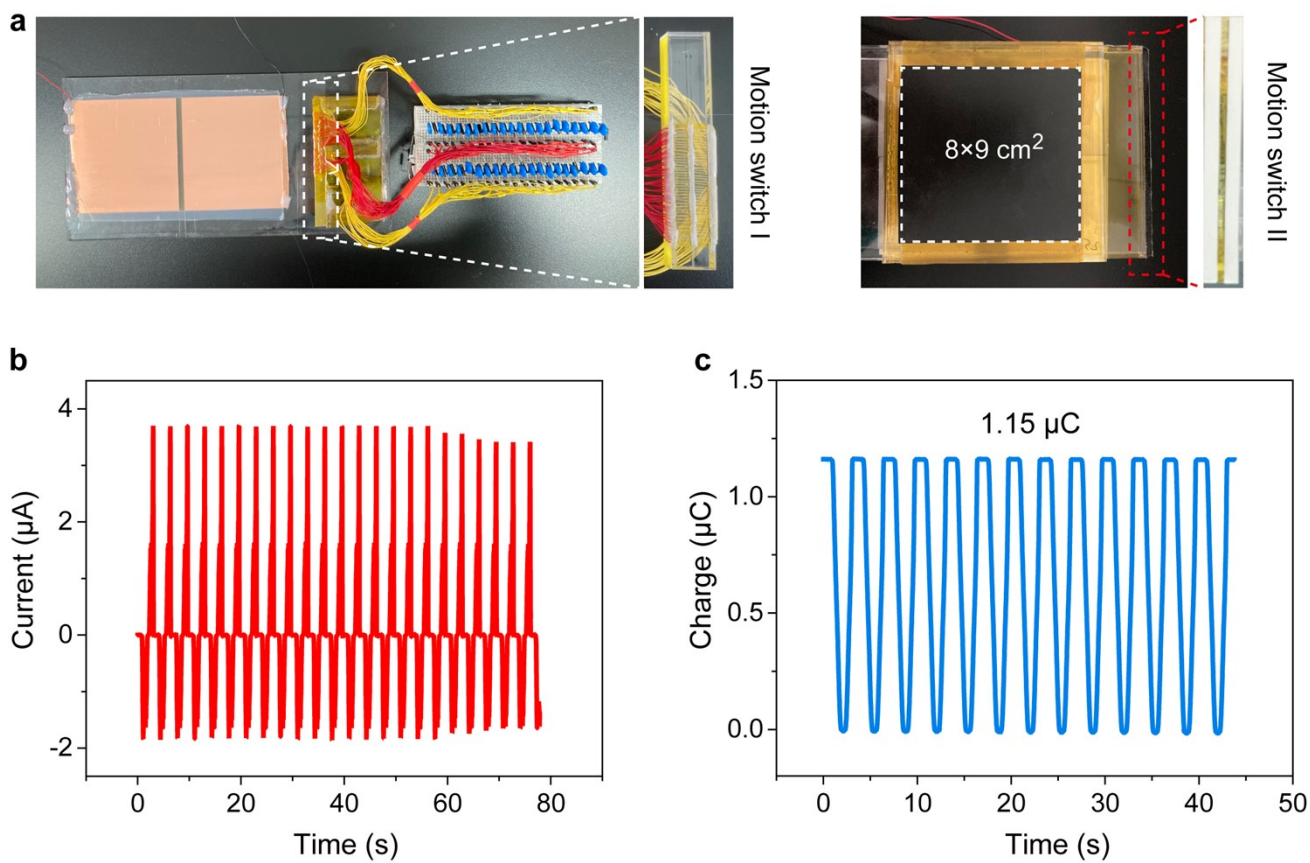


Fig. S8. **a**, Optical photograph of a TENG with equivalent fractal circuit (EFC), which consist of 40 capacitors and 40 diodes. **b,c**, Short-circuit current and output charge of the TENG only.

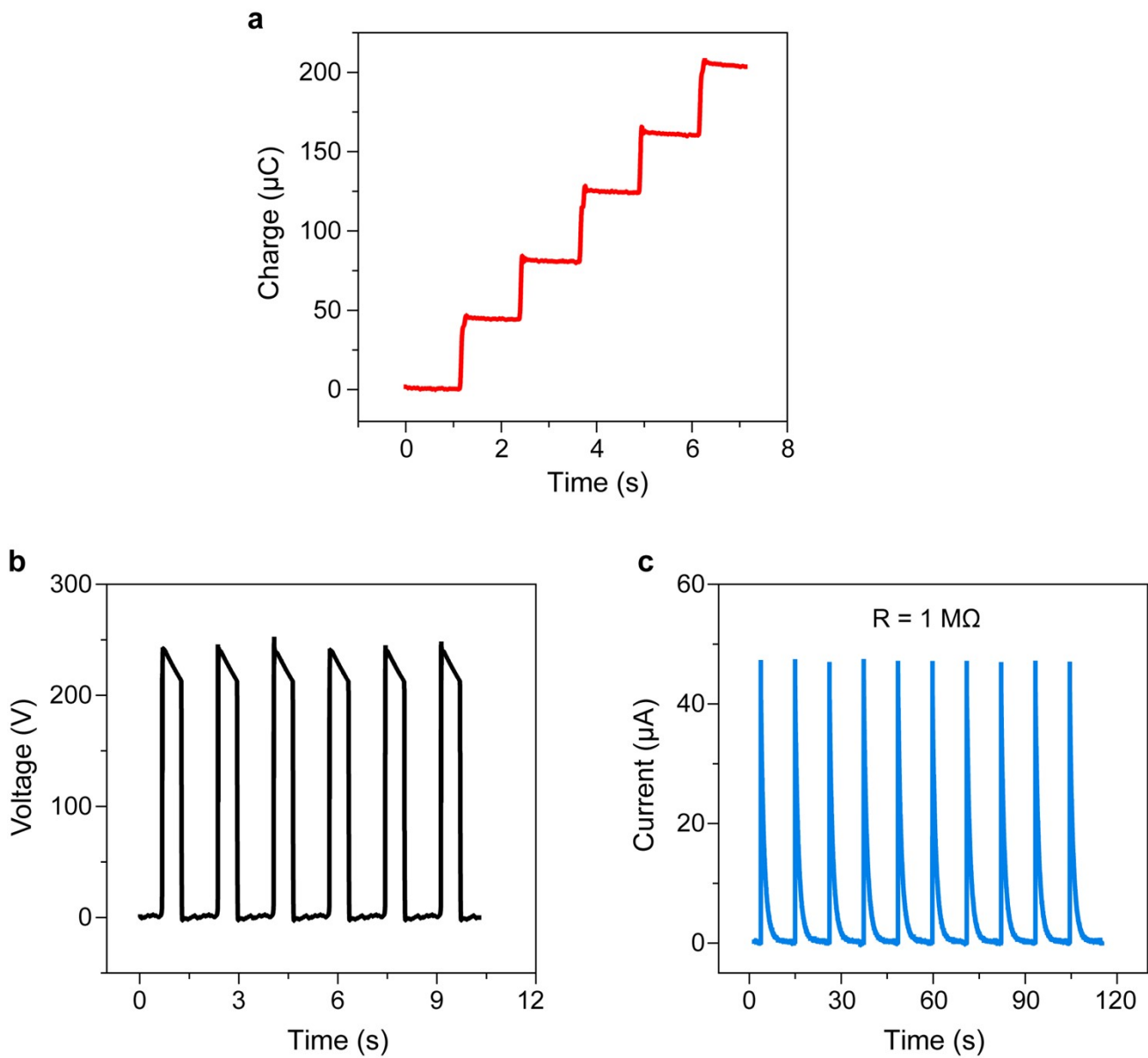


Fig. S9. The output performance of a TENG with optimized EFC (40 capacitors with 22 nF). (a) Output charge, (b) Open-circuit voltage, and (c) Output current (load resistance R of 1 $\text{M}\Omega$) of the TENG with EFC.

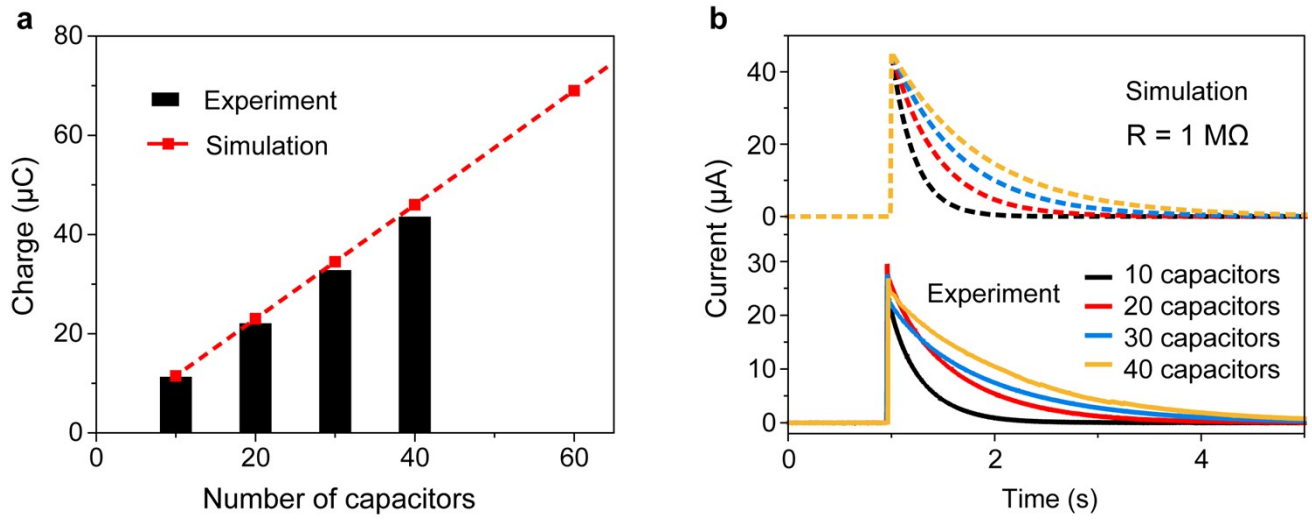


Fig. S10. The influence of capacitor numbers in the EFC. a,b, Output charge and output current of a TENG with EFC versus the number of capacitors (22 nF) in the EFC from simulation and experiment.

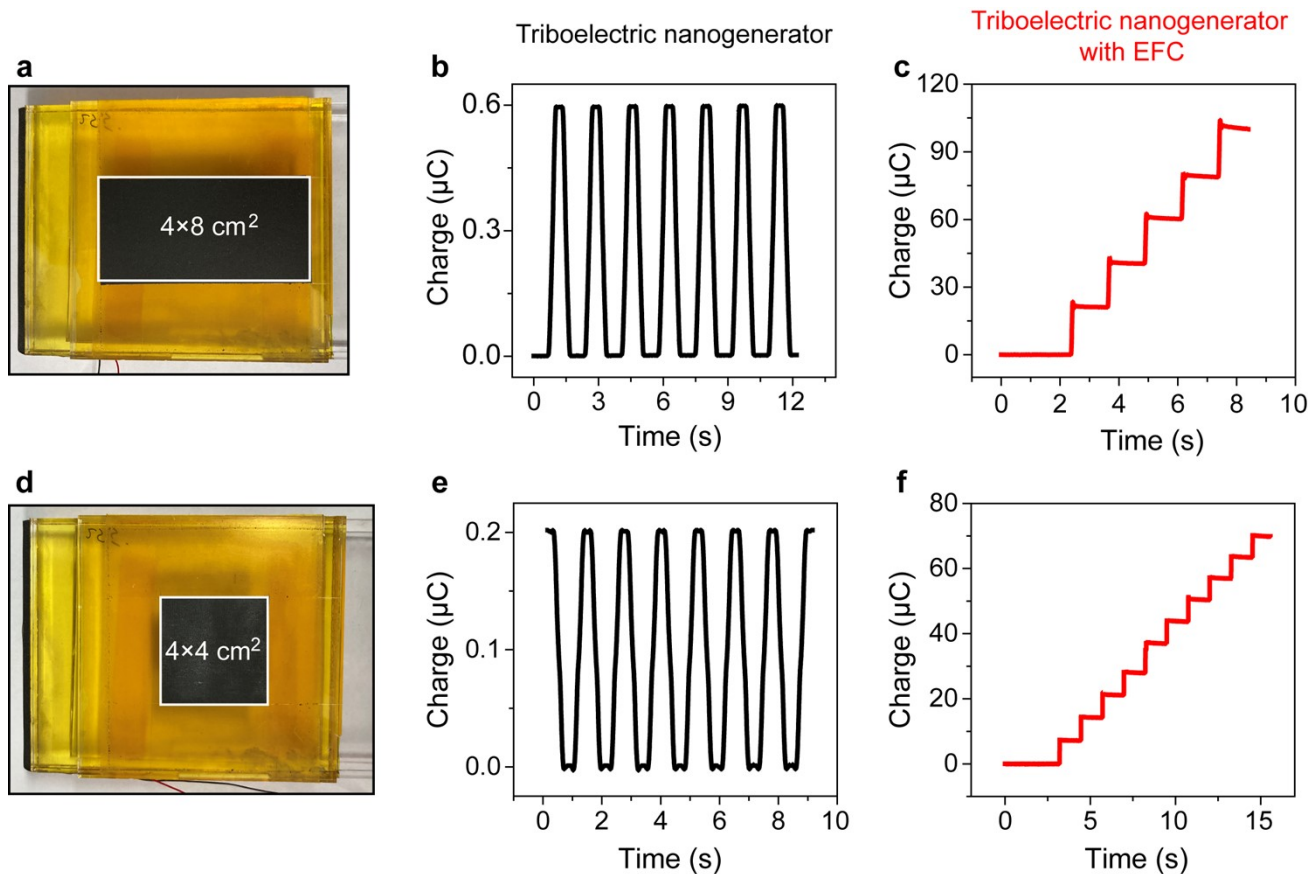


Fig. S11. The universality of EFC. (a) The optical photo and (b) output charge of a TENG with effective area of $4 \times 8 \text{ cm}^2$, and corresponding (c) output charge of the TENG with optimized EFC. (d) The optical photo and (e) output charge of a TENG with effective area of $4 \times 4 \text{ cm}^2$, and corresponding (f) output charge of the TENG with optimized EFC.

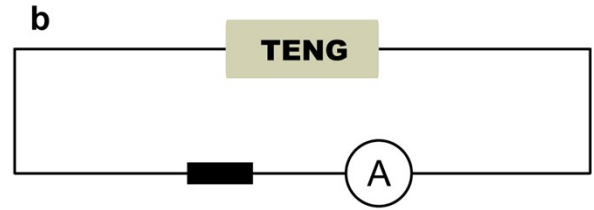
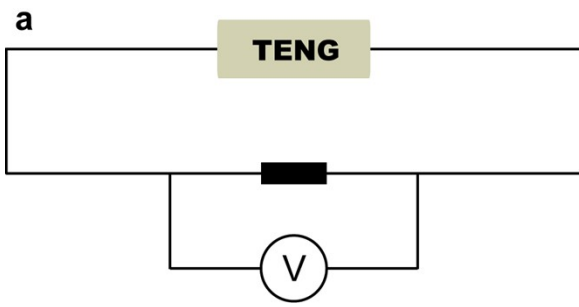


Fig. S12. The circuit for measuring the current across resistance. **a**, The circuit for measuring the current across resistance, which is higher than 1 mA. The current is calculated from the voltage across the resistance measured by an oscilloscope (Tektronix, MDO 3024). **b**, The circuit for measuring the current across the resistance, which is lower than 1 mA. The current is directly measured by Keithley 6514 electrometer.

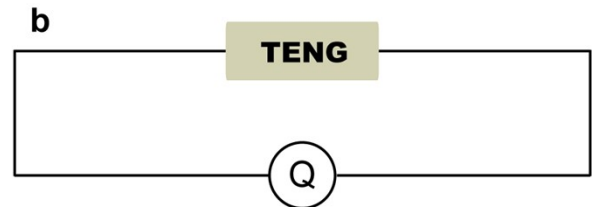
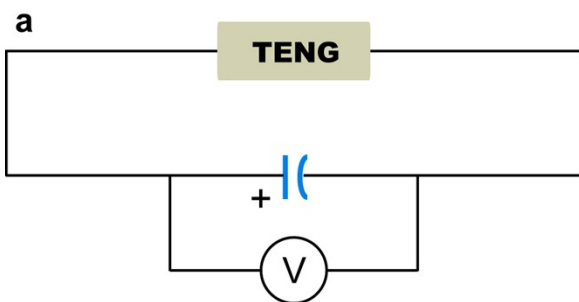


Fig. S13. The circuit for measuring output charge. **a**, The circuit for measuring the output charge that is higher than 20 μC , which is calculated from the voltage of the electrolytic capacitor with capacitance of 10 μF . And the voltage is measured by Keithley 6514 electrometer. **b**, The charge (lower than 20 μC) is measured by Keithley 6514 electrometer (measuring range of 0-20 μC).

Movie S1. Measurement of output charge of the FSNG with 40 fractal units.

Movie S2. The process of LED straps (rated power of 120 W) lighted by the FSNG.

Movie S3. The continuous working process of a digital vernier driven by the FSNG.

Movie S4. The continuous working process of a temperature hygrometer driven by the FSNG.

Movie S5. The process of a dozen LEDs lighted for more than 10 seconds by the FSNG during one cycle of operation.